PROCEEDINGS OF SCIENCE

A Model for Soft and Hard Interactions based on the CGC/Saturation Approach

E. Gotsman[*a], **E. Levin** [ab] **and I. Potashnikova**[b]
[a] *School of Physics and Astronomy, Tel Aviv University*
69978 Tel Aviv, Israel
[b] *Departamento de Fisica, Universidad Tecnica Federico Santa Maria Avda. Espana, 1680*
Valparaiso, Chile
E-mail: gotsman@post.tau.ac.il, leving@post.tau.ac.il, irina.potashnikova@usm.cl

A model based on the CGC/saturation approach and the BFKL Pomeron, was initially constructed to describe soft interactions at LHC energies. This model has now been extended to also describe hard interactions at HERA energies. The model also successfully describes inclusive production, rapidity and angular correlations over a wide range of energies. We outline the formalism and compare the model predictions with the relevant experimental data.

XIII Quark Confinement and the Hadron Spectrum - Confinement2018
31 July - 6 August 2018
Maynooth University, Ireland

[*] Speaker.

PoS(Confinement2018)179

1. Introduction

At first sight the soft interactions at high energies occur at long distances where one needs to use non-perturbative QCD. Since our poor understanding of non-perturbative QCD, we are doomed to use pure phenomenological approaches, which might or might not reflect the features of our microscopic theory: QCD. The scattering amplitude in perturbative QCD is governed by the exchange of the BFKL Pomeron [1]. It has been shown that the interaction of the BFKL Pomerons generates a new dimensional scale: saturation momentum $Q_s(Y)$[2, 3, 4, 5], which increases with energy (see Figure 1), and produces a system of partons, which are non-perturbative by nature, however, the QCD coupling in this system of partons is small ($\bar{\alpha}_S(Q_s) \ll 1$). This new phase in QCD: Colour Glass Condensate(CGC), can be treated theoretically (see book [6] for a review). The main idea of our approach to soft interactions at high energies, is that the high energy amplitudes are determined by this CGC phase. In other words, we assume that the main contribution to the soft interaction at high energies stems from the perturbative BFKL Pomerons, and their interactions, which can be treated theoretically, using the CGC approach. However, we cannot avoid using some phenomenology, which reflects the structure of the hadrons. In terms of the BFKL Pomerons we have to introduce a phenomenological description for the interaction of the scattering hadrons with the BFKL Pomerons. This description is a source of the non-perturbative dimensional parameters, which reflect the long distance physics. We have extended our model to also describe electron-proton interactions at HERA energies, and show that the BFKL Pomeron successfully describes both soft [7, 8] and hard interactions [9] at high energy.

2. Scattering near the unitarity limit

In the Regge limit of pQCD, when $s \gg \Lambda_{hard}$, as the energy increases, the parton density becomes more dense, and the scattering amplitude A(s,t) grows. As long as densities are not too high, the growth is described by the BFKL evolution equation. The density becomes higher as A(s,t) $\to$ 1, and one enters the "saturation" regime (see Figure 1), where the BFKL evolution fails. Non-linearities lead to saturation + unitarization of A(s,t). The Balitsky-Kovchegov equation [10], is the simplest and most accurate way to describe the saturation regime of QCD. It is non-linear and resums QCD fan diagrams in the LLA (leading log approximation).

3. Phenomenological input

A deficiency that has to be overcome, is the fact that the BFKL Pomeron does not lead to shrinkage of the diffractive peak, and has no slope for the Pomeron trajectory. This can be cured by introducing a non-perturbative correction at large impact parameter, which also assures satisfying the Froissart-Martin bound for σ_{tot} [13].

In our model we fix the large b (impact parameter) behaviour by assuming that the saturation momentum has the following form:

$$Q_s^2(b,Y) = Q_{0s}^2(b,Y_0)e^{\lambda(Y-Y_0)} and Q_{0s}^2(b,Y_0) = (m^2)^{(1-\frac{1}{\bar{\gamma}})}[S(b,m)]^{\frac{1}{\bar{\gamma}}} \tag{3.1}$$

with $S(b,m) = \frac{m^2}{2\pi}e^{-mb}$ and $\bar{\gamma} = 0.63 = 1 - \gamma_{cr}$

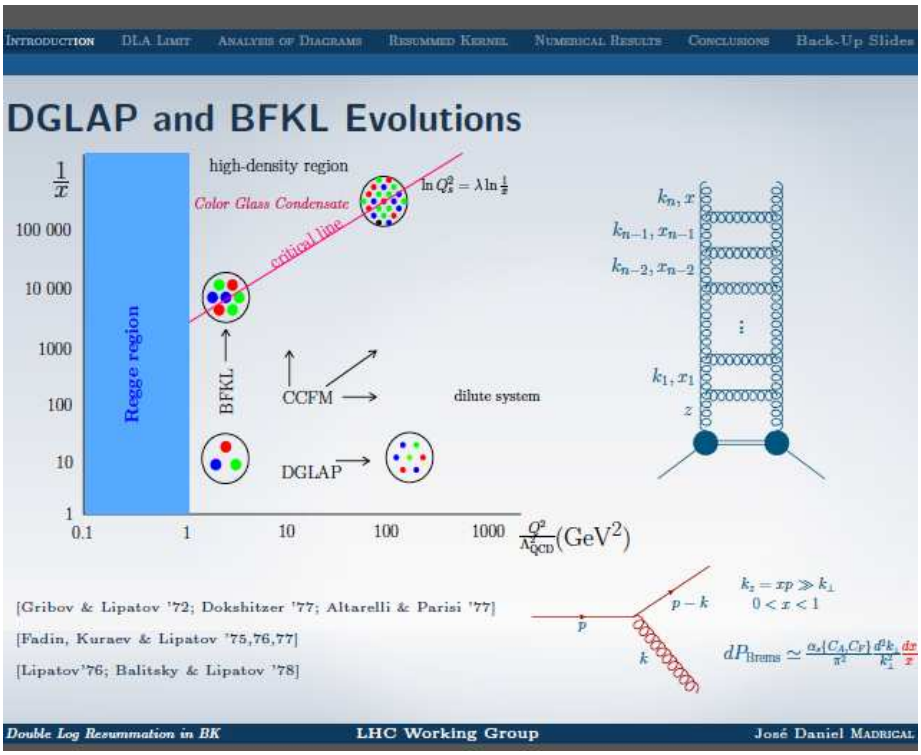

Figure 1: Guide to the various evolution regions (from a talk by Jose Daniel Madrigal) [11]

The parameter $\lambda = \bar{\alpha}_S \chi(\gamma_{cr}) / (1 - \gamma_{cr})$, in leading order of perturbative QCD ($\lambda = 0.2$ to 0.3)

The parameter m is introduced to describe the large b behaviour, it determines the typical sizes of dipoles inside the hadron. There are two additional scales m_1 and m_2, which describe two typical sizes in the proton wave function. One can associated these with: (i) the distance between the constituent quarks; size of the proton $R_p \approx \frac{1}{m_1}$. (ii) m_2 can be associated with the size of the constituent quark; $R_q \approx \frac{1}{m_2}$. Altinoluk et al [14] have proved the equivalence of the CGC/saturation approach and the BFKL Pomeron calculus for a wide range of rapidities $Y \leq \frac{2}{\Delta_{\rm BFKL}} \ln\left(\frac{1}{\Delta^2_{\rm BFKL}}\right)$.

4. Dressed Pomeron in the MPSI approximation

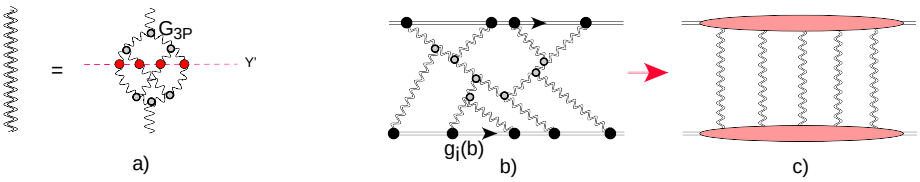

Figure 2: a) Dressed Pomeron in MPSI approximation. b) reduces to c) after integration over the positions of G_{3P} in rapidity. Wavy lines describe BFKL Pomerons, double wavy show dressed Pomerons, red blobs denote the amplitude for dipole-dipole interactions. The grey blobs stand for triple Pomeron vertices, while black blobs show the hadron-Pomeron vertex $g_i(b)$.

Since the typical rapidity is $O(Y-Y_i) \approx \frac{1}{\Delta_{BFKL}}$, only large Pomeron loops with rapidity $O(Y)$ contribute at high energies $\rightarrow$ can sum such loops using MPSI approximation [12].

For the BFKL Pomeron $\lambda = 4.88\bar{\alpha}_s$ while $\Delta_{BFKL} = 4ln2\bar{\alpha}_s \approx 0.2$.

The resulting Green function of the Dressed Pomeron is given by:

$$G_{I\!P}^{\rm dressed}(Y-Y_0,r,R,b) = a^2\left\{1-\exp\left(-T(Y-Y_0,r,R,b)\right)\right\} + 2a(1-a)\frac{T(Y-Y_0,r,R,b)}{1+T(Y-Y_0,r,R,b)} + (1-a)^2\left\{1-\exp\left(\frac{1}{T(Y-Y_0,r,R,b)}\right)\frac{1}{T(Y-Y_0,r,R,b)}\Gamma\left(0,\frac{1}{T(Y-Y_0,r,R,b)}\right)\right\} \quad (4.1)$$

$$T(Y-Y_0,r,R,b) = \frac{\bar{\alpha}_S^2}{4\pi}G_{I\!P}(z\rightarrow 0) = \phi_0\left(r^2Q_s^2(R,Y,b)\right)^{1-\gamma_{cr}} = \phi_0 S(,mb)\,e^{\lambda(1-\gamma_{cr})Y} \quad (4.2)$$

where $T(Y-Y_0,r,R,b)$ denotes the BFKL Pomeron in the vicinity of the saturation scale.

z = $ln(r^2Q_s^2(b,Y))$, a = 0.65 and $\gamma_{cr} \approx 0.37$

In addition to describe the vertices of the hadron-Pomeron interaction, we need to introduce four constants: g_i and m_i $(i=1,2)$.

$g_i(b) = g_i S_{I\!P}(m_i,b)$ with $S_{I\!P}(m_i,b) = \frac{m_i^3 b}{4\pi}K_1(m_i b)$

$S_{I\!P}(m_i,b) \xrightarrow{\text{Fourier image}} (\frac{m_i^2}{q^2+m_i^2})^2$

This has the same form as the electromagnetic form factor of the proton and leads to the correct e^{-mb} behaviour at large impact parameter and q^{-4}, at large q, as required by QCD.

The opacity is given by

$$\Omega_{i,k}(Y;b) = \int d^2b' \frac{g_i(b')\,g_k(b-b')\,\bar{G}_{I\!P}^{\rm dressed}(Y)}{1+1.29\bar{G}_{I\!P}^{\rm dressed}(Y)\left[g_i(b')+g_k(b-b')\right]}, \quad (4.3)$$

where $\bar{G}_{I\!P}^{\rm dressed}(Y) = \int d^2b''\,G_{I\!P}^{\rm dressed}(Y;b'')$.

5. Basic formalism for two channel model

Following Good-Walker [15] the observed physical hadronic and diffractive states are written

$$\psi_h = \alpha\Psi_1+\beta\Psi_2; \quad \psi_D = -\beta\Psi_1+\alpha\Psi_2; \qquad \text{where} \qquad \alpha^2+\beta^2=1 \quad (5.1)$$

Functions ψ_1 and ψ_2 form a complete set of orthogonal functions $\{\psi_i\}$ which diagonalize the interaction matrix **T**

$$A_{i,k}^{i'k'} = <\psi_i\psi_k|\mathbf{T}|\psi_{i'}\psi_{k'}> = A_{i,k}\delta_{i,i'}\delta_{k,k'}.$$

The unitarity constraints can be written as

$$2{\rm Im}A_{i,k}(s,b) = |A_{i,k}(s,b)|^2 + G_{i,k}^{in}(s,b) \quad (5.2)$$

At high energies a simple solution to this equation is

$$A_{i,k}(s,b) = i\left(1-\exp\left(-\frac{\Omega_{i,k}(s,b)}{2}\right)\right) \quad (5.3)$$

λ	ϕ_0	$g_1\,(GeV^{-1})$	$g_2\,(GeV^{-1})$	$m(GeV)$	$m_1(GeV)$	$m_2(GeV)$	β
0.38	0.0019	110.2	11.2	5.25	0.92	1.9	0.58

Table 1: Values of parameters obtained from the fit to the soft interaction data.

$$G^{in}_{i,k}(s,b) = 1 - \exp\left(-\Omega_{i,k}(s,b)\right). \tag{5.4}$$

$G^{in}_{i,k}(s,b)$ denotes the contribution of all non-diffractive inelastic processes.

For the combinations of amplitudes corresponding to the different observables see [7]. The values of the parameters determined from the fit to the soft interaction data [7, 8] is given in Table 1.

6. Deep inelastic (Hard) scattering

To introduce "Hard Interactions" we consider DIS: where the physical observables are:

The transverse and longitudinal DIS cross sections

$$\sigma_{T,L}(Q,Y) \;=\; 2\int d^2b\, N_{T,L}(Q,Y;b) \tag{6.1}$$

and the inelastic structure function

$$F_2(Q,Y) \;=\; \frac{Q^2}{4\pi^2\alpha_{\rm e.m.}}\Big\{\sigma_T + \sigma_L\Big\} \tag{6.2}$$

Q denotes the photon virtuality, and $Y = \ln(1/x_{Bj})$,

x_{Bj} is the Bjorken x, and b denotes the impact parameter for the scattering of the colourless dipole of size r with the proton.

The observables for DIS can be re-written using

$$N_{T,L}(Q,Y;b) \;=\; \int\frac{d^2r}{4\pi}\int_0^1 dz\,|\Psi^{\gamma^*}_{T,L}(Q,r,z)\,|^2\,N(r,Y;b) \tag{6.3}$$

$N(r,Y;b)$ denotes the scattering amplitude of the dipole and z is the fraction of energy carried by quark. b is the impact parameter for the scattering of the colourless dipole of size r with the proton.

$|\Psi^{\gamma^*}_{T,L}(Q,r,z)\,|^2$ is the probability to find a dipole of size r in a photon with the virtuality Q, with transverse or longitudinal polarization. This splits the calculation of the hard scattering amplitude into two stages:

a) calculation of the wave function and b) estimates of the dipole scattering amplitude.

The wave functions are:

$$(\Psi^*\Psi)^{\gamma^*}_T = \frac{2N_c}{\pi}\alpha_{\rm em}\sum_f e_f^2\left\{\left[z^2+(1-z)^2\right]\varepsilon^2K_1^2(\varepsilon r) + m_f^2K_0^2(\varepsilon r)\right\} \tag{6.4}$$

$$(\Psi^*\Psi)^{\gamma^*}_L = \frac{8N_c}{\pi}\alpha_{\rm em}\sum_f e_f^2Q^2z^2(1-z)^2K_0^2(\varepsilon r) \tag{6.5}$$

and $\varepsilon^2 = m_f^2 + z(1-z)Q^2$.

Since we take into account the contribution of the heavy c-quark we introduce a correction due to large mass of this quark: $x_{Bj} \to x_{Bj}\left(\frac{1}{1+\frac{4m_c^2}{Q^2}}\right)$ or $Y_c = Y - \ln\left(1+4m_c^2/Q^2\right)$

In describing the saturation phenomena and fitting the strong interaction data, we assumed that the QCD coupling is frozen at some value of momentum $\mu_{\rm soft}$.

For DIS we take into account the running QCD coupling: Hence,

$$F_2(Q,Y) = \frac{Q^2}{4\pi^2\alpha_{\rm e.m.}}\left\{\frac{\bar{\alpha}_S\left(Q^2\right)}{\bar{\alpha}_S\left(\mu^2\right)}\sigma^{\rm light\,q}(Q,Y) + \frac{\bar{\alpha}_S\left(Q^2+4m_c^2\right)}{\bar{\alpha}_S\left(\mu^2\right)}\sigma^{\rm charm\,q}(Q,Y_c)\right\} \tag{6.6}$$

where μ denotes the typical mass of the soft strong interaction $\mu \sim 1\,GeV$ and

$$\frac{\bar{\alpha}_S\left(Q^2\right)}{\bar{\alpha}_S\left(\mu^2\right)} = \frac{1}{1+\beta\bar{\alpha}_S\left(\mu^2\right)\ln\left(Q^2/\mu^2\right)} \tag{6.7}$$

with $\beta = 3/4$.

We considered the strong interaction data (see [8, 16] for details) for energies $W \geq 0.546\,TeV$, while the experimental data from HERA (see [9] for details) were measured for lower energies $10.7 \leq W \leq 301$ GeV. Therefore, it is necessary to include secondary reggeons which provide a substantial contribution. They are parametrized as follows:

$$\sigma_{I\!R}(Q,Y) = \int\frac{d^2r}{4\pi}\left\{(\Psi^*\Psi)_T^{\gamma^*} + (\Psi^*\Psi)_L^{\gamma^*}\right\}A_{I\!R}\,r^2\left(\frac{Q^2}{x_{Bj}Q_0^2}\right)^{\alpha_{I\!R}(0)-1} \tag{6.8}$$

with $Q_0 = 1\,GeV$.

The final expression for F_2 is :

$$F_2(Q,Y) = \frac{Q^2}{4\pi^2\alpha_{\rm e.m.}}\left\{\frac{\bar{\alpha}_S\left(Q^2\right)}{\bar{\alpha}_S\left(\mu^2\right)}\sigma^{\rm light\,q}(Q,Y) + \frac{\bar{\alpha}_S\left(Q^2+4m_c^2\right)}{\bar{\alpha}_S\left(\mu^2\right)}\sigma^{\rm charm\,q}(Q,Y_c) + \sigma_{I\!R}(Q,Y)\right\} \tag{6.9}$$

The values of the parameters determined from a fit to the HERA data , are given in Table 2.

7. Parameters of the DIS fit to data

We introduce an additional set of new parameters for DIS: m_q-mass of the light quark, which we assume to be of the order of the constituent quark mass ($\sim 300\,MeV$), and the mass of charm quark ($m_c = 1.2 \div 1.5\,GeV$). μ which we believe will be of the order of 1 GeV, and in addition we introduce two new parameters $A_{I\!R}$ and $\alpha_{I\!R}(0)$ for the secondary Reggeon contribution. The values of the parameters, given in Table 2, are determined from a fit to the relevant HERA data [19], and compared to the DIS data in (see Fig.3).

8. Conclusions

We have reviewed our model for high energy soft and hard interactions. We show our results for the parameters determined for the soft and for the combined (soft + hard) data in Table 3 and

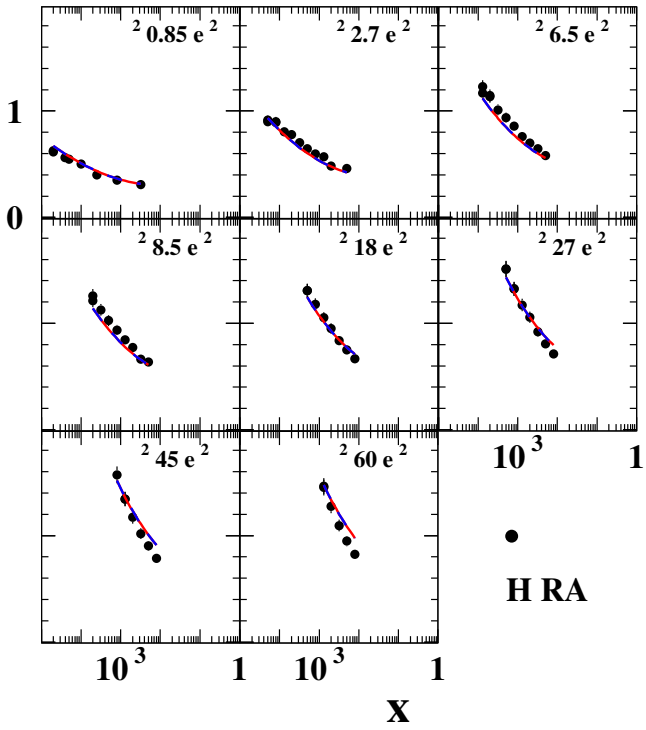

Figure 3: F_2 versus x at fixed Q. The red curve corresponds to Fit I (strong interactions only), while the blue curve describes Fit II (strong interaction plus DIS). Data is taken from HERA [19]

.

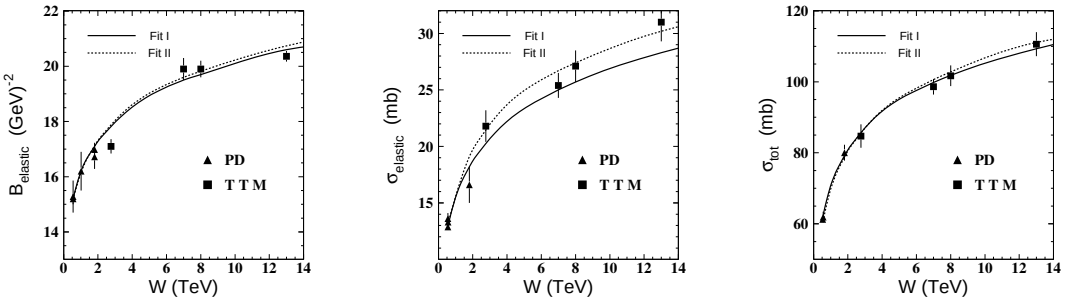

Figure 4: The energy behaviour of σ_{tot}, σ_{el} and the slope B_{el} in our model. Fit I (soft data only) and Fit II (soft + hard data). Data are taken from Ref.[19]

Fit	$m_q(GeV)$	$m_c(GeV)$	$\alpha_S(\mu)$	μ (GeV)	$A_{I\!R}(GeV^2)$	$\alpha_{I\!R}(0))$
I	0.3	1.25	0.263	1.2	2.34	0.55
II	0.2	1.2	0.34	1.25	5.44	0.56

Table 2: Values of parameters obtained from fit to DIS data: Fit I refers to values obtained for new parameters associated with F_2 while keeping parameters for the soft data fixed. Fit II refers to a joint fit to soft and DIS data [19].

W (TeV)	σ_{tot} (mb)	σ_{el}(mb) (mb)	B_{el} (GeV^{-2})	single $\sigma_{\rm sd}^{\rm smd}$ (mb)	diffraction $\sigma_{\rm sd}^{\rm lmd}$ (mb)
0.576	62.3(60.7)	12.9(13.1)	15.2(15.17)	5.64(4.12)	1.85(1.79)
0.9	69.2(68.07)	15(15.05)	16(15.95)	6.254.67)	2.39(2.35)
1.8	79.2(78.76)	18.2(19.1)	17.1(17.12)	7.1(5.44)	3.35(3.28)
2.74	85.5(85.44)	20.2(21.4)	17.8(17.86)	7.6(5.91)	4.07(4.02)
7	99.8(100.64)	25(26.7)	19.5(19.6)	8.7(6.96)	6.2(6.17)
8	101.8(102.8)	25.7(27.4)	19.7(19.82)	8.82(7.1)	6.55(6.56)
13	109.3(111.07)	28.3(30.2)	20.6(20.74)	9.36(7.64)	8.08(8.11)
14	110.5(111.97)	28.7(30.6)	20.7(20.88)	9.44(7.71)	8.34(8.42)
57	131.7(134.0)	36.2(38.5)	23.1(23.0)	10.85(9.15)	15.02(15.01)

Table 3: Predicted values of cross-sections and $B_{elastic}$ for different values of energy. The results of fit II, are shown in parenthesis.

Fig.4. We have demonstrated that the Colour Glass Condensate/saturation approach, which is the only reasonable candidate for the effective QCD theory at high energies, can be viewed as the basis for the description of typical hard and soft processes. This occurs, as the CGC/saturation approach predicts that at high energy, the system of partons is produced with the typical new scale: saturation momentum, which increases with energy. This means that short distance interactions contribute to the processes, which previously we used to consider as being due to long distances physics.

This statement is supported by the description of three type of the processes described by our model: quasi elastic scattering [7, 8, 19], multi particle generation [17, 18, 19] and deep inelastic scattering [9, 19] . This is the only model on the market today which is successful in doing so.

References

[1] E. A. Kuraev, L. N. Lipatov, and F. S. Fadin, *Sov. Phys. JETP* **45**, (199) 1977; Ya. Ya. Balitsky and L. N. Lipatov, *Sov. J. Nucl. Phys.* **28**, (1978) 1.

[2] L. V. Gribov, E. M. Levin and M. G. Ryskin, *Phys. Rep.* **100** (1983) 1.

[3] E. M. Levin and M. G. Ryskin, *High-energy hadron collisions in QCD*, *Phys. Rept.* **189**, (1990) 267.

[4] A. H. Mueller and J. Qiu, *Nucl. Phys.* **B268** (1986) 427.

[5] L. McLerran and R. Venugopalan, *Phys. Rev.* **D49** (1994) 2233, 3352; **D50** (1994) 2225; **D53** (1996) 458; **D59** (1999) 09400.

[6] Yuri V Kovchegov and Eugene Levin, *Quantum Chromodynamics at High Energies*, Cambridge Monographs on Particle Physics, Nuclear Physics and Cosmology, Cambridge University Press, 2012.

[7] E. Gotsman, E. Levin and U. Maor, *Eur. Phys. J. C* **75** (2015) 18 [hep-ph/1408.3811].

[8] E. Gotsman, E. Levin and U. Maor, *Eur. Phys. J. C* **75** (2015) 179 [hep-ph/1502.05202].

[9] E. Gotsman, E. Levin and I. Potashnikova, *Phys. Lett. B* **781** (2018) 155 [hep-ph/1712.06992].

[10] I. Balitsky, [hep-ph/9509348]; *Phys. Rev.* **D60**, (1999) 014020 [hep-ph/9812311]; Y. V. Kovchegov, *Phys. Rev.* **D60**, (1999) 034008, [hep-ph/9901281].

[11] J. D. Madrigal *"Double Log Summation in BK"*, [Talk at LHC Working Group, CERN 2015].

[12] A. H. Mueller and B. Patel, *Nucl. Phys.* **B425** (1994) 471. A. H. Mueller and G. P. Salam, *Nucl. Phys.* **B475**, (1996) 293. [hep-ph/9605302]. G. P. Salam, *Nucl. Phys.* **B461** (1996) 512; E. Iancu and A. H. Mueller, *Nucl. Phys.* **A730** (2004) 460 [hep-ph/0308315]; [hep-ph/0309276].

[13] M. Froissart, *Phys. Rev.* **123** (1961) 1053; A. Martin, *Scattering Theory: Unitarity, Analitysity and Crossing* Lecture Notes in Physics, Springer-Verlag, Berlin-Heidelberg-New-York, 1969.

[14] T. Altinoluk, A. Kovner, E. Levin and M. Lublinsky, *JHEP* **1404** (2014) 075 [hep-ph/1401.7431].

[15] M. L. Good and W. D. Walker, *Phys. Rev.***120** (1960) 1857.

[16] E. .Gotsman, E. Levin and I. Potashnikova, *Eur. Phys. J. C* **77** (2017) 632, [hep-ph/1706.07617].

[17] E. Gotsman, E. Levin and U. Maor, inclusive *Phys. Lett. B* **746** (2015) 154 [hep-ph/1503.04294].

[18] E. Gotsman, E. Levin and U. Maor, *Eur. Phys. J. C* **75** (2015) 518 [hep-ph/1508.04236].

[19] M. Tanabashi et al. (Particle Data Group), *The Review of Particle Physics (2018)*, *Phys. Rev.* **D 98**, 030001 (2018).

[20] E. Gotsman, E. Levin and I. Potashnikova, *Phys. Lett. B* in print [hep-ph/1807.06459].